Dec. 2024
Volume 4
Issue 2

Advances in Medical, Pharmaceutical and Dental Research Journal (AMPDR)- ISSN 2812-4898
http://dx.doi.org/10.21622/AMPDR.2024.04.2.923

A Computational Assessment Of Alkaloids Targeting The Plant Homeodomain In Pygopus2: Inhibitory Potential And Drug-Like Properties

[1*]Zechariah Oresanya, [2]Olaide Odesanya, [3]Ibrahim Olaniyi, [4]Christian Agbojo, [5]God's Will Eleanya and [6]Rahmon Kanmodi

[1:4] Department of Chemistry, Faculty of Science, Lagos State University, Lagos State, Nigeria
[5] Department of Biochemistry, Faculty of Science, Lagos State University, Lagos State, Nigeria.
[6] Department of Oncological science, University of Utah, Utah, United States.

Emails: zechariaholuwadamilola@gmail.com*, Odesanyaolaide@gmail.com, Adetunjiibrahimolaniyi@gmail.com, agbojochristian2002@gmail.com, phillipsuche00@gmail.com, rahmonilesanmi@gmail.com

Received on, 10 July 2024 - Accepted on, 20 August 2024 - Published on, 18 September 2024

ABSTRACT:

Pygopus2 (Pygo2) is a component of the Wnt signaling pathway, crucial for β-catenin-mediated transcription during normal development. Overexpression of Pygo2 has been linked to various human cancers, including lung, colon, and brain cancers. The plant homeodomain (PHD) finger in Pygo2 intercalates with the methylated histone 3 (H3K4me) tail and the HD1 domain of B-cell lymphoma 9 protein (BCL9), which binds to β-catenin. This interaction highlights the PHD finger as a promising target for designing anti-cancer drugs. Despite the importance of this protein in numerous cancers, no approved drug currently targets it. In this study, the researchers used in silico techniques to identify alkaloids with favourable PHD binding affinities compared to standard compounds. Three alkaloids—discorhabdin W (9.7 Kcal/mol), topsentin A (9.1 Kcal/mol), and dragmacidin A (9.0 Kcal/mol)—emerged as the best candidates, exhibiting stronger binding effects compared to JBC117 (9.2 Kcal/mol), a compound that has been shown to inhibit cancer cell proliferation both ex vivo and in vivo. They also exhibited compliance with Lipinski's rule, promising drug-like properties, and relatively low toxicity. Molecular dynamics simulations of the three high-affinity protein-ligand complexes revealed considerable conformational flexibility, hinge regions, and low eigenvalues, indicating stable and flexible molecular motions. Based on the findings from this study, these three alkaloids have the potential to be developed as anticancer lead compounds targeting the PHD finger of Pygo2.

Graphical Abstract:

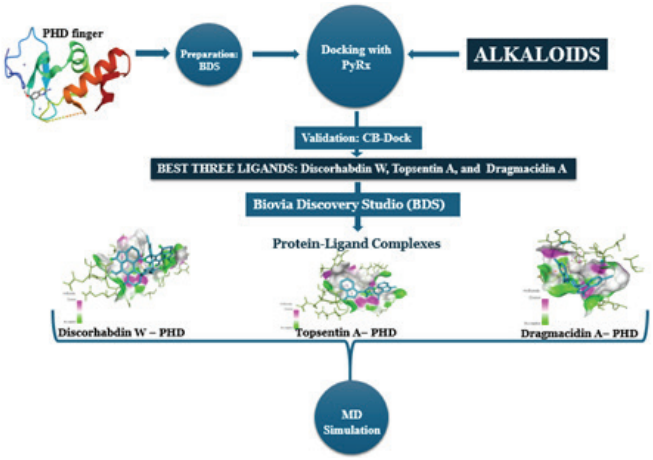

KEYWORDS:

Discorhabdin W, Binding affinities, Molecular dynamics, Lipinski, Hinge regions.

1. Introduction

Mutations in genes encoding central components of the Wnt signaling pathway and destruction complex lead to nuclear β-catenin accumulation and contribute to tumor initiation and progression (1–3). Pygopus2 (Pygo2) is a Wnt signaling component essential for β-catenin-mediated transcription during normal development (4). The overexpression of Pygo2 has been documented in several cancers including those of the breast, cervical, hepatic, lung, intestinal, and brain

cancers. Therefore, understanding and targeting Pygo2 may have translational significance in various cancer types (5).

Pygo2 recognizes modified histone 3 (H3K4me) tails by their cysteine-rich zinc-binding plant homeodomain (PHD) and the HD1 domain of B-cell lymphoma 9 protein (BCL9), an adaptor protein that directly binds to β-catenin (3,6,7). Consequently, the PHD is essential for β-catenin-dependent transcriptional regulation in both normal and malignant tissues. Given the critical role of the PHD domain in Pygo2 function, the interaction interfaces with its binding partners may represent promising targets for inhibiting the oncogenic function of β-catenin (4). However, despite the significance of this protein in various human cancers, no approved drug has been developed against it. Therefore, it is crucial for the medicinal chemist to identify lead inhibitors or compounds to target the PHD domain in Pygo2.

Plants are recognized as rich sources of bioactive compounds used in cancer treatment (8). Approximately 35% of all anticancer drugs developed for cancer management between 1981 and 2014 were derived from plant sources, with alkaloids constituting a highly diverse category known for their various pharmacological properties, including anticancer effects. These active agents utilize diverse molecular mechanisms to block, suppress, and inhibit the metastasis of cancer cells (9). Their biological activities are mainly due to their interactions with various molecular targets, such as biomembranes, proteins, DNA topoisomerase, etc. (10). They interact with proteins through various mechanisms, impacting protein conformation and stability. These interactions are characterized by binding constants, conformational changes in proteins, and thermodynamic parameters indicating the spontaneity and driving forces of the binding process (11–13). Their modes of action include the alteration of enzymes or specific transcription factors crucial at various stages of cancer progression. Additionally, they act as inhibitors of the STAT-3 and PI3K/Akt signaling pathways (14). Alkaloids have a proven track record in cancer treatment, with several alkaloid-based drugs currently in clinical use, demonstrating the practical effectiveness of this class of compounds. Examples include vincristine, vinblastine (15), docetaxel, and paclitaxel (Taxol) (16).. Alkaloids have shown potential in inhibiting key proteins involved in diseases like COVID-19, diabetes, cancer, etc. Studies have highlighted the efficacy of alkaloids in targeting proteins such as α-glucosidase in diabetes management (17), and VEGF and VEGFR in cancer treatment (18). Mondal *et al*., (2019) reported that liriodenine an alkaloid isolated from *Enicosanthellum pulchrum,* inhibited the proliferation of CAOV-3 human ovarian cancer cells through induction of apoptosis via the mitochondrial signaling pathway and blocked cell-cycle progression at the S-phase. It caused the upregulation of Bax and downregulation of Bcl-2 and survivin proteins (19).

In this study, We aim to identify alkaloid-based lead compounds targeting the PHD finger, the histone-binding surface of Pygo2, for the first time, leveraging the favourable anticancer potential of alkaloids. Using a computational approach, we evaluated the binding affinities and druglike properties of various alkaloid ligands with known anticancer properties for the protein. The binding affinities were then compared with those of JBC117, a compound proven to bind the PHD domain of Pygo2 and inhibit cancer cell proliferation both ex vivo and in vivo, as reported by Ali *et al.* (2016) and Zhu *et al,* (2023). The alkaloids with favourable binding affinities were then subjected to molecular dynamics simulation for further evaluations.

2. METHODOLOGY

2.1 Identification and Preparation of 4UP5

The structure 4UP5 was retrieved from the Research Collaboratory for Structural Bioinformatics (RCSB) Protein Data Bank (PDB) (https://www.rcsb.org/), an online repository that provides free access to thousands of protein structures (20). The protein was prepared following the method described by Kanmodi, *et al*. (2023) (21). Briefly, the 3D crystal structure of the Pygo2 PHD domain in complex with the cocrystallized chemical compound (PDB ID: 4UP5, resolution: 1.65 Å) was downloaded in PDB format and prepared using Biovia Discovery Studio 4.5 software (https://discover. 3ds.com/discovery-studio-visualizer-download) to remove water molecules and hetatoms, and to add polar hydrogen atoms. Before molecular docking, the PDB format of the protein was converted to the Protein Data Bank, Partial Charge (Q), and Atom Type (T) format (PDBQT) using the integrated Autodock wizard tool in PyRx.

2.2 Identification and Preparation of Ligands for Docking

The 3D structures of hundred (100) alkaloids of various classes with reported anticancer properties (19)(22) were downloaded in structured data format (SDF) from PubChem (https://pubchem.ncbi.nlm.nih.gov); a free, user-friendly database storing millions of chemical compounds (23). These alkaloids and their respective CIDs are shown in Table 1. Additionally, the researchers downloaded the 3D-SDF format of the co-crystallized ligand 6-methoxy-1,3-benzothiazol-2-amine (CID: 15630) of 4UP5 and JBC117 (CID: 46955251) from PubChem. Before molecular docking, energy minimization was carried out, thereby converting the ligands from SDF to PDB format; lastly, they converted them to PDBQT format.

Advances in Medical, Pharmaceutical and Dental Research Journal (AMPDR)- ISSN 2812-4898
http://dx.doi.org/10.21622/AMPDR.2024.04.2.923

2.3 Molecular Docking

AutoDock Vina, an integral component of the PyRx software package (https://pyrx.sourceforge.io/), was utilized to perform multiple ligand dockings against 4UP5 Cavity-detection guided Blind Docking (CB-Dock; http://clab.labshare.cn/cb-dock/php/index.php) prediction was used to validate the researchers' docking protocols and results. Like PyRx, CB-Dock uses AutoDock Vina for blind molecular docking, enabling the prediction of protein-ligand binding affinities.(21). PyRx, a computer-based drug discovery software, is capable of screening compound libraries against potential therapeutic targets and is one of the few docking software packages suitable for multiple docking. With optimized multithreading capabilities, the integrated AutoDock Vina in PyRx demonstrates significantly enhanced speed and efficiency. It internally determines grid charges and establishes the docking space (24). Following the preparation of the ligands and protein, the docking process was executed using the Vina Wizard. The docking area encompassing the PHD was selected, with the grid box dimensions set to 37 Å x 31 Å x 30 Å. The parameter settings for AutoDock Vina included an exhaustiveness value of 8 and a maximum of 20 generated binding modes. Other optional settings were left at their default values. Subsequently, the binding energy scores and root mean square deviation (RMSD) values of the docked complexes were generated and downloaded in CSV format. Additionally, the equation ki = exp (-△G/RT) was used to calculate the inhibition constant. Where △G is the binding energy output from PyRx in Kcal/mol, R is 1.987 cal/mol/K and T is 298.15K.

2.4 Physicochemical, Dug-like properties and Toxicity Evaluation

The in silico physicochemical properties of the top three hits from the docking study, assessed using Lipinski's rule of five and Jorgensen's rule of three, were predicted using the QikProp module of Schrödinger and SwissADME. The best three ligands with the lowest binding energies were selected, and their canonical SMILES were generated and uploaded to the SwissADME (http://www.swissadme.ch) server for analysis of their drug-like characteristics and other pharmacokinetic parameters. SwissADME is a free online tool for assessing the pharmacokinetics, drug-likeness, and medicinal chemistry friendliness of small molecules (25). Furthermore, to assess the toxicity of these PHD-binding ligands, their canonical smiles were uploaded to the ProTox-II (https://tox.charite.de/) server. The server utilizes molecular similarity and machine-learning models to predict 61 toxicity endpoints, including acute toxicity, organ toxicity, clinical toxicity, molecular-initiating events (MOEs), adverse outcomes (Tox21 pathways), and various other toxicological endpoints and off-target toxicities. All ProTox 3.0 models are validated on independent external datasets and have demonstrated strong performance (26). Lastly, AMETlab 3.0 was utilized to determine the probable inhibitory effects of the ligands on hERG (human ether-a-go-go-Related Gene).

2.5 Molecular Dynamics Simulation

Molecular dynamics (MD) simulations of protein-ligand complexes were performed using CABS-flex V 2.0 (http://biocomp.chem.uw.edu.pl/CABSflex2) and the iMOD server (iMODS) (http://imods.chaconlab.org), as described by Sumera *et al.* (2022) (27). CABS-flex was used to assess the structural flexibility (RMSF) of the protein. The simulation time was set to 10 ns, while other parameters were left at their default values. Root-mean-square fluctuations (RMSFs) were obtained based on the MD trajectory or NMR ensemble with default options.

To evaluate the stability and molecular motion of the docked protein–alkaloid complexes, MD simulations were carried out using the iMOD server. iMODS analyzed the structural dynamics of the docking complexes and determined the molecular motion. The stability of the protein–alkaloid (the best three alkaloids; discorhabdin W, dragmacidin A, and topsentin A) complexes were assessed based on deformability, B-factor, eigenvalues, variance, covariance map, and elastic network. Docked PDB files were uploaded to the iMODS server with the atomic model selection set at HA and other parameters set to default.

2.6 Analysis of Ligand–Protein Interaction

After docking with the target protein, the three ligands with the lowest binding energies and highest binding affinities were selected to examine the associated protein-ligand complex structures and bond interactions. Hydrogen bonding and other interactions between the ligands and amino acid residues of the protein-ligand complexes were visualized using Biovia Discovery Studio software. Biovia Discovery Studio was also employed to generate 2D structures illustrating the interactions within the protein-ligand complexes.

3. RESULTS

3.1 Molecular Docking

The pharmacological pipeline benefits significantly from in silico modeling, including reduced failure rates, shorter clinical trial durations, and lower research and development costs (28). Given the demonstrated anticancer activities of various alkaloid ligands, the researchers assessed the binding energies of these alkaloids with the PHD, as

shown in Table 1. All the ligands showed high PHD binding affinity compared to the cocrystallized ligand. The three ligands with the best PHD binding affinities were selected and their binding affinities and inhibition constants were compared to standard molecules (JBC117 and cocrystallized ligand) as presented in Table 2. It has been demonstrated that discorhabdin W inhibits the PHD domain more effectively than dragmacidin A, topsentin A, and the standard compounds.

Table 1: Binding energies (△G) in Kcal/mol of the interactions of the 100 alkaloids with the PHD and their reported anticancer properties (29)(22)(19).

S/N	Ligands	CID	Rmsd		Binding Affinity (Kcal/mol)	Cell lines/substrate/enzyme/in vivo; Effects
			lb	ub		
1	Tambjamine A	135610508	0.0	0.0	-5.4	A549; Induction of necrosis
2	Mimosamycin	4198	0.0	0.0	-5.6	P388; Induction of cytotoxicity
3	Indicine N-Oxide	280564	0.0	0.0	-5.7	HeLa; increase apoptosis
4	Cribrostatin 1	10330480	0.0	0.0	-5.8	P388; Induction of cytotoxicity
5	Noscapine	275196	0.0	0.0	-5.8	several cancer cells; cell-cycle arrest at mitosis
6	Arborescidine D	378619	0.0	0.0	-5.9	in vitro activity against the growth of KB human buccal carcinoma cells
7	19(S)-Heyneanine	44566752	0.0	0.0	-5.9	human laryngeal carcinoma (Hep-2) cells; increased apoptosis
8	Piperlongumine	637858	0.0	0.0	-5.9	prostate cancer cell by inhibition of NF-κB and decrease in the expression of IL-6, IL-8, MMP-9, and intercellular adhesion molecule 1 (ICAM-1)
9	Tambjamine I	381030	0.0	0.0	-5.9	SW900; imbalance in cellular ion homeostasis
10	Clivorine	21606566	0.0	0.0	-6.1	L-02 (human fetal hepatocyte); Induction of p38 mitogen-activated protein kinase
11	Pibocin B	9975094	0.0	0.0	-6.1	Mouse Ehrlich carcinoma cells; cytotoxic activity
12	Tambjamine K	135934866	0.0	0.0	-6.1	H460; mitochondrial dysfunction
13	Sanguilutine	356660	0.0	0.0	-6.2	mitotic catastrophe in LNCaP and PC-3 (prostate cancer) and HeLa (cervical cancer) cells
14	Tryptoline	107838	0.0	0.0	-6.2	renal cancer cell; decreased DNA topoisomerases and DNA synthesis
15	Tylophorine	92114	0.0	0.0	-6.2	HONE-1 (epithelial tumor); cell-cycle arrest at G1 phase
16	Voacangine	73255	0.0	0.0	-6.2	HeLa (human laryngeal carcinoma (Hep-2) cells); increased apoptosis
17	Antofine	639288	0.0	0.0	-6.3	Col2 (Colon cancer cells); Cell cycle arrest in the G2/M phase
18	Arnottianamide	3085181	0.0	0.0	-6.3	Caspase 3 stimulant and MMP9 expression inhibitor
19	Coronaridine	6426909	0.0	0.0	-6.3	(HeLa-human laryngeal carcinoma (Hep-2) cells); increased apoptosis
20	Pretazettine	73360	0.0	0.0	-6.3	L5178 MDR (murine leukemia); Antiproliferative effect, cell-cycle arrest at G0/G1 phase
21	Rohitukine	13422573	0.0	0.0	-6.3	A549; Apoptosis
22	Sampangine	387195	0.0	0.0	-6.3	HL-60; Apoptosis
23	Clathrodin	5388709	0.0	0.0	-6.4	Clathrodin; Induction of cytotoxicity
24	Dercitin	130774	0.0	0.0	-6.4	solid human lung cancer line and a mouse leukemia line; inhibits a variety of cultured cell clones
25	Dibromophakellstatin	10500579	0.0	0.0	-6.4	KM20L2 (colon cancer), H-460 (lung cancer); cell growth inhibitory activity
26	Harman	5281404	0.0	0.0	-6.4	Calf-thymus DNA; decreased DNA topoisomerases and DNA synthesis
27	Harmine	5280953	0.0	0.0	-6.4	Calf-thymus DNA; decreased DNA topoisomerases and DNA synthesis

Advances in Medical, Pharmaceutical and Dental Research Journal (AMPDR)- ISSN 2812-4898
http://dx.doi.org/10.21622/AMPDR.2024.04.2.923

28	Homoharringtonine	285033	0.0	0.0	-6.4	Leukemia; TRAIL-induced necroptosis
29	Hypoestestatin 2	126663	0.0	0.0	-6.4	P-388; Induction of cytotoxicity
30	Norchelerythrine	443719	0.0	0.0	-6.4	P-388 cell line; cytotoxicity against several cell lines
31	Trisphaeridine	443684	0.0	0.0	-6.4	MDR (murine leukemia); cell-cycle arrest at sub-G1 phase
32	Carboxymethyldihydrochelerythrine	13946324	0.0	0.0	-6.5	Potency against A549, Hela, SMMC-7721, and EJ.
33	Chelerythrine	2703	0.0	0.0	-6.5	HEK-293 (human embryonic kidney cells); Apoptosis
34	Harmalol	3565	0.0	0.0	-6.5	Calf-thymus DNA; decrease DNA topoisomerases
35	Oxymatrine	114850	0.0	0.0	-6.5	non-small cell lung cancer (NSCLC); inhibition of STAT5
36	Pericalline	6436240	0.0	0.0	-6.5	P-388 (mouse leukemia); Induction of cytotoxicity
37	Vallesiachotamine	5384527	0.0	0.0	-6.5	KB; Induction of cytotoxicity
38	Harmaline	3564	0.0	0.0	-6.6	Calf-thymus DNA; decreased DNA topoisomerases and DNA synthesis
39	Meridianin E	9995236	0.0	0.0	-6.6	Antiproliferative activity in several cancer cell lines; potent and selective inhibition of CDK-1 and CDK-5
40	Neocryptolepine	390526	0.0	0.0	-6.6	HL-60 (promyelocytic leukemia); cell-cycle arrest at G2/M phase
41	Ellipticine	3213	0.0	0.0	-6.7	MCF-7; Induction of cytotoxicity
42	Discorhabdin L	135451013	0.0	0.0	-6.7	P-388 cells; Induction of cytotoxicity
43	Mappianine B	137347205	0.0	0.0	-6.7	MGC-803 (human gastric cancer), Bel-7404 (human hepatoma cells), A549, NCI–H460 (lung carcinoma cells), HepG2 (human liver carcinoma); Cytotoxicity
44	6-Acetonyldihydroavicine	101212618	0.0	0.0	-6.8	-
45	Berberine	2353	0.0	0.0	-6.8	DLD-1 (colon cell line); inhibition of COX-2 transcriptional activity
46	Cryptolepine	82143	0.0	0.0	-6.8	HL-60 (promyelocytic leukemia); cell-cycle arrest at G2/M phase
47	Hernandezine	72343	0.0	0.0	-6.8	A549; Induction of autophagy
48	Jorumycin	9849761	0.0	0.0	-6.8	MEL-28 (Human malignant melanoma); Induction of cytotoxicity
49	Brucine	442021	0.0	0.0	-6.9	PC-9 (lung cancer); Antiproliferative effect
50	Chelidonine	197810	0.0	0.0	-6.9	HepG2; Induction of G2/M arrest
51	Discorhabdin D	135846979	0.0	0.0	-6.9	P-388 cells; Induction of cytotoxicity
52	Fascaplysin	73293	0.0	0.0	-6.9	HL-60; Apoptosis, activates the PARP-1 cleavage
53	Isoplysin A	135465870	0.0	0.0	-6.9	L-1210 (mouse lymphocytic leukemia); Induction of cytotoxicity
54	Oxynitidine	97597	0.0	0.0	-6.9	
55	Tylophorinidine	161749	0.0	0.0	-6.9	Dihydrofolate reductase from L. *leichmannii*; decreased dihydrofolate reductase
56	6-Methoxyspirotryprostatin B	24900164	0.0	0.0	-7	A-549; Induction of cytotoxicity
57	9-Methoxycamptothecin	123617	0.0	0.0	-7	P-388; induction of cytotoxicity and topoisomerase inhibition
58	Arctigenin	64981	0.0	0.0	-7	CaCo-2 (Caucasian colon adenocarcinoma); Induction of cytotoxicity
59	Fangchinoline	73481	0.0	0.0	-7	T24 and 5637 (Urinary bladder cancer); Apoptosis
60	Kuanoniamine A	390989	0.0	0.0	-7	solid human lung cancer line and a mouse leukemia line; cytotoxic activity
61	Prodigiosin	135455579	0.0	0.0	-7	Human oral squamous carcinoma cells (OECM1 and SAS); cell cycle arrest in G0/G1 phase

62	18-Oxotryprostatin A	24900162	0.0	0.0	-7.1	A-549; Induction of cytotoxicity
63	Discorhabdin G	135515105	0.0	0.0	-7.1	P-388 cells; Induction of cytotoxicity
64	Leucosolenamine A	16104874	0.0	0.0	-7.1	C-38 cells; Induction of cytotoxicity
65	Liriodenine	10144	0.0	0.0	-7.1	CAOV-3 (ovarian cancer); accumulation of G2 cyclin (B1)
66	Madangamine A	9980274	0.0	0.0	-7.1	P388 (leukemia); in vitro cytotoxicity
67	Piperine	638024	0.0	0.0	-7.1	HT-29; Apoptosis, cell-cycle arrest at G1
68	Sanguinarine	5154	0.0	0.0	-7.1	BxPC-3 (adenocarcinoma of the pancreas); Induction of cytotoxicity
69	Sewarine	5458504	0.0	0.0	-7.1	KB; Induction of cytotoxicity
70	2-Bromoleptoclinidinone	378074	0.0	0.0	-7.3	L 1210 murine leukemia, P388, etc.; excellent in vitro cytotoxicity
71	Cycleanine	121313	0.0	0.0	-7.3	Ovcar-8 and A2780 (Ovarian cancer); Apoptosis
72	Scutebarbatine A	45110781	0.0	0.0	-7.3	A549; Apoptosis
73	Tetrahydrosecamine	169527	0.0	0.0	-7.3	P-388); Induction of cytotoxicity
74	Stylopine	6770	0.0	0.0	-7.5	HCT116, MCF-7; inhibition of AKR1C3
75	14-Hydroxyterezine D	24900165	0.0	0.0	-7.6	HL-60; Induction of cytotoxicity
76	Fumiquinazoline G	10247811	0.0	0.0	-7.6	P388 cells; Induction of cytotoxicity
77	Arcyriaflavin A	5327723	0.0	0.0	-7.7	K562 cell line; Apoptosis
78	Deoxytubulosine	165003	0.0	0.0	-7.7	Dihydrofolate reductase from *Lactobacillus leichmannii*; decease dihydrofolate reductase activity
79	Haliclonadiamine	10316977	0.0	0.0	-7.7	six human cancer cell lines; inhibition of cell proliferation
80	Pyrayafoline D	375148	0.0	0.0	-7.7	HL-60; Apoptosis
81	Fumiquinazoline	11247802	0.0	0.0	-7.8	Isolate from marine-derived fungus Aspergillus sydowii PFW-13; Induction of cytotoxicity
82	Fumiquinazoline F	10089772	0.0	0.0	-7.8	Isolate from marine-derived fungus Aspergillus sydowii PFW-13; Induction of cytotoxicity
83	Papuamine	10248478	0.0	0.0	-7.8	human cancer cell lines; accumulation of lymphoma U937 cells at sub-G1 phase
84	Neferine	159654	0.0	0.0	-7.9	Human cells hTERT-RPE1, HEK-293, and Hela; cell cycle arrest at G1
85	Nortopsentin C	456386	0.0	0.0	-7.9	P-388 cells; Induction of cytotoxicity
86	Wakayin	9973710	0.0	0.0	-7.9	human colon tumor cell line; inhibiting topoisomerase II enzyme by damaging the DNA
87	1′,2′,3′,4′-Tetradehydrotubulosine	21668793	0.0	0.0	-8	KB; Induction of cytotoxicity
88	Luteoalbusin A	71497282	0.0	0.0	-8	SF-268, MCF-7, NCI-H460, and Hep G-2 cell lines; Induction of cytotoxicity
89	Mahanine	36689305	0.0	0.0	-8	HL-60; Apoptosis, loss of mitochondrial membrane potential
90	Luteoalbusin B	71497283	0.0	0.0	-8.1	SF-268, MCF-7, NCI-H460, and Hep G-2 cell lines; Induction of cytotoxicity
91	Bisleuconothine A	46881778	0.0	0.0	-8.2	A549; Induction of autophagy
92	Zanthomuurolanine	44567548	0.0	0.0	-8.3	Antineoplastic and apoptosis agonist
93	Moschamine	5969616	0.0	0.0	-8.5	CaCo-2; Induction of cytotoxicity
94	Biemnadin	163156431	0.0	0.0	-8.7	KB and L1210 cells in vitro; exhibited cytotoxicity
95	Fumiquinazoline C	11339719	0.0	0.0	-8.7	Isolate from marine-derived fungus Aspergillus sydowii PFW-13; Induction of cytotoxicity
96	Nortopsentin B	456387	0.0	0.0	-8.8	P-388; Induction of cytotoxicity
97	Nortopsentin A	179268	0.0	0.0	-9	P-388; Induction of cytotoxicity

Advances in Medical, Pharmaceutical and Dental Research Journal (AMPDR)- ISSN 2812-4898
http://dx.doi.org/10.21622/AMPDR.2024.04.2.923

98	Dragmacidin A	11260315	0.0	0.0	-9	P388 and A549 tumor cell lines; inhibition of growth
99	Topsentin A	183527	0.0	0.0	-9.1	Antiproliferative activity against human bronchopulmonary cancer cells (NSCLC-N6)
100	Discorhabdin W	135466418	0.0	0.0	-9.7	P-388 cells; Induction of cytotoxicity
Standard Molecules						
101	6-Me-thoxy-1,3-Benzo-thiazol-2-Amine	15630	0.0	0.0	-4.8	
102	(JBC117)	46955251	0.0	0.0	-9.2	

Table 2: The binding energy of the best three compounds and standard compounds binding PHD assessed by PyRx and CB-Dock.

Ligands	Canonical smiles	Binding Affinities (Kcal/mol)		Inhibition constant (Ki)
		PyRx	CB-Dock	
Discorhabdin W	C1CN=C2C3=C1C=NC3=C(C4=C-2C5(C=CN4)C=C(C(=O)C=C5SSC6=C-C(=O)C(=CC67C=CNC8=C7C9=NCCC1=C-9C(=C8O)N=C1)Br)Br)O	-9.7	-9.5	108.58 nM
Topsentin A	C1=CC=C2C(=C1)C(=CN2)C3=CN=C(N3)C(=O)C4=CNC5=CC=CC=C54	-9.1	-9.0	252.51 nM
Dragmacidin A	CN1CC(NCC1C2=CNC3=C2C=CC(=C3)Br)C4=CNC5=C4C=CC(=C5)Br	-9.0	-9.1	213.29 nM
Standard molecules				
JBC117	CC1=CC2=C(C=C1)C(=CN2)C(CN3C-CC4(CC3)CC(C5=C(O4)C6=CC=CC=C-6C=C5)O)O	-9.2	-9.1	213.29 nM
6-methoxy-1,3-ben-zothiazol-2-amine	COC1=CC2=C(C=C1)N=C(S2)N	-4.8	-5	216.07 µM

3.2 Analysis of Physicochemical, Drug-like Properties, and Toxicity of the Best Three Ligands

The projected gastrointestinal absorption (GIA) of the top three alkaloids is summarized in Table 3. Topsentin A and dragmacidin A demonstrated a high probability of absorption in the gastrointestinal tract, whereas discorhabdin W showed a low absorption probability. This suggests that topsentin A and dragmacidin A could be effectively absorbed following oral administration (30). The blood-brain barrier (BBB), composed of brain microvascular endothelial cells, separates the brain from the bloodstream (31). The ability of the ligands to cross the BBB was evaluated, with the results also presented in Table 3. The data indicate that both topsentin A and discorhabdin W could not cross the BBB, which may be beneficial as it minimizes the risk of adverse effects on the central nervous system (CNS) (32).

Table 3: Physicochemical, Pharmacokinetic, and Toxicity Analysis of the best three Alkaloids.

Ligands	Topsentin A	Discorhabdin W	Dragmacidin A
Physicochemical Properties			
MW	326.35	826.54	488.22
Num of H-bond Acceptor	2	8	2
Num of H-bond Donors	3	4	3
Molar Refractivity	97.61	223.92	125.65
Pharmacokinetics			
GI absorption	High	Low	High
BBB permeant	No	No	Yes
P-gp substrate	Yes	Yes	Yes

CYP1A2 Inhibitor	Yes	No	Yes
CYP2C19 Inhibitor	Yes	No	Yes
CYP2C9 Inhibitor	No	Yes	No
CYP2D6 Inhibitor	Yes	No	Yes
CYP3A4 Inhibitor	Yes	No	Yes
Toxicity			
Class	4	6	4
LD50 (mg/kg)	1264	6000	313
Hepatotoxicity	Active	Inactive	Inactive
Nephrotoxicity	Inactive	Inactive	Inactive
Cardiotoxicity (hERG blocker)	0.36	0.429	0.614

Legend: MW: Molecular weight; BBB: Blood-brain barrier; P-gp: Permeability glycoprotein; CYP: Cytochrome P450; GI: Gastrointestinal.

Understanding how different compounds interact with cytochromes P450 (CYPs) is crucial. This superfamily of isoenzymes is responsible for metabolic biotransformation processes such as hydroxylation of aliphatic and aromatic carbons, epoxidation of aromatic or olefinic double bonds, heteroatom oxidation and dealkylation, and dehydrogenation, which are essential for drug elimination (33). It is estimated that 50 to 90 percent of pharmaceutical compounds are substrates of one of the five main CYP isoforms: CYP1A2, CYP2C19, CYP2C9, CYP2D6, and CYP3A4 (34). Ensuring that drug-metabolizing CYPs remain uninhibited is a key consideration in new drug development (35). Inhibition of these isoenzymes can lead to decreased clearance and accumulation of the drug or its metabolites, a major cause of pharmacokinetics-related drug-drug interactions that may result in toxic or undesirable effects (36). Although dragmacidin A and topsentin A inhibit most of these enzymes, discorhabdin W inhibits just one, CYP2C9, indicating a high probability of metabolic conversion and good bioavailability after oral administration (31).

The role of a compound as a P-glycoprotein (P-gp) inhibitor or substrate is crucial in drug development, especially in addressing multidrug resistance (MDR) in cancer therapy. Compounds that are substrates for P-gp are actively transported out of cells, reducing their intracellular concentration and, consequently, their therapeutic efficacy (37). This suggests that the efflux activity of P-gp may impact the alkaloids.

Table 4: Oral Bioavailability of the Best Three Ligands

S/N	Ligands	Lipinski's Rule of Five	Jorgensen's Rule of 3
1.	Discorhabdin W	Yes; 1 violations: MW>500	Yes; 2 violations: metab > 7and Logs < -5.7
2.	Topsentin A	Yes; 0 violation	Yes; 0 violation
3.	Dragmacidin A	Yes; 0 violation	Yes; 0 violation

The oral bioavailability of the best three alkaloids was evaluated based on their physicochemical features. Lipinski's filter (38) considers the following criteria: a molecular weight of 500 or less, no more than 10 hydrogen bond acceptors, no more than 5 hydrogen bond donors, and an MLOGP (lipophilicity) of less than 4.15. Compounds with two or more violations are likely to exhibit low oral bioavailability (39). Therefore, the ligands are predicted to be orally bioavailable based on Lipinski's filter Table 4. According to Jorgensen's rule of three, a compound is more likely to be orally bioavailable if it meets all or some criteria such as logS > -5.7, PCaco-2 > 22 nm/s, and having fewer than 7 primary metabolites. Discorhabdin W, with 8 primary metabolites, slightly exceeds this threshold. However, based on Jorgensen's rule, the ligands are still predicted to be orally bioavailable.

3.3 PHD-Ligand Interactions

The interaction of the ligands with the PHD domain is presented in both 2D and 3D shown in Figure 1. The non-covalent interactions exhibited by the complexes include alkyl, conventional hydrogen bond, carbon-hydrogen bond, pi-alkyl, pi-anion, pi-sulfur bond, pi-pi stacked, and van der Waals interactions. The discorhabdin W-PHD complex showed an unfavourable acceptor-acceptor interaction. The acceptor-acceptor proximity within the complex may cause electrostatic repulsion between their lone pairs of electrons, potentially destabilizing the complex. This could reduce binding affinity or prevent optimal binding configurations.

The interaction between the cocrystallized ligand – PHD and JBC117-PHD was also examined in Discovery Studio as presented in Figure 1D and 1E respectively. In the former, the sulfur of the benzothiazole ring faces the solvent, like the methoxy group at C6, which faces away from the HD1-binding surface of PHD. This is consistent with the reports of Miller *et al.* (2014); the methoxy group is the most exposed group of the ligand and the only one that does not contact PHD at all (40). However, while they observed hydrogen bond formation at ASP 380, the researchers report the formation of multiple hydrogen bonds between the

Advances in Medical, Pharmaceutical and Dental Research Journal (AMPDR)- ISSN 2812-4898
http://dx.doi.org/10.21622/AMPDR.2024.04.2.923

best binding pose of the cocrystallized ligand and the amino acid residues of PHD including GLU 372, ALA 373, and 375.

By examining the interactions in Figure 1, it may be concluded that all the ligands bind in the same site because of the identical amino acid residues such as THR 370, TYR 366, ALA 343, ASN 338, and GLN 341which may correspond to a strong pocket binding position. Since the cocrystallized ligand binds at similar residues – GLU 372 and ALA373 – as discorhabdin W and judging from the presence of VAL 376 reported by Ali *et al.* (2016), this binding site resembles the PHD – HD1 domain described by Miller *et al.* (2014) as the "benzothiazole cleft".

A

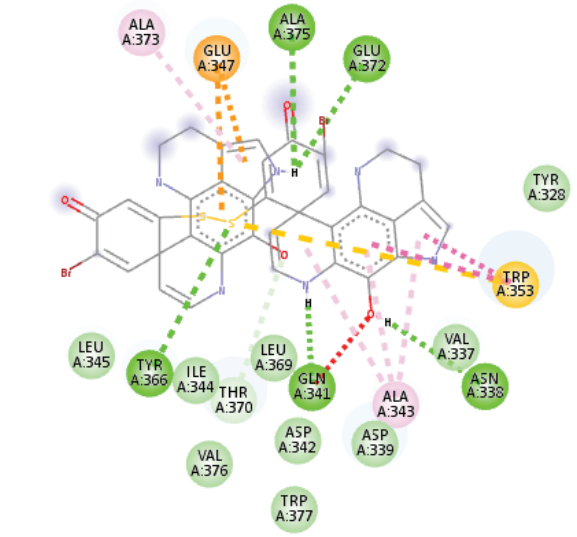

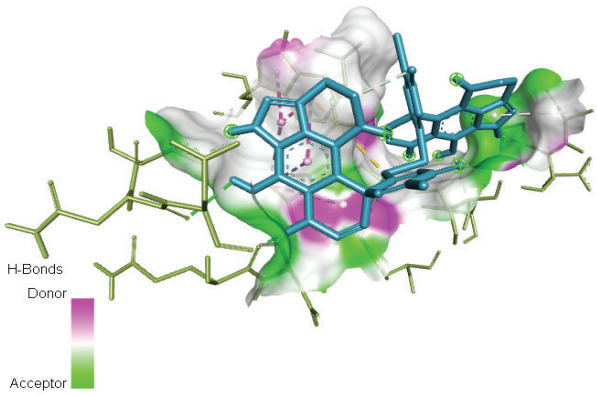

B

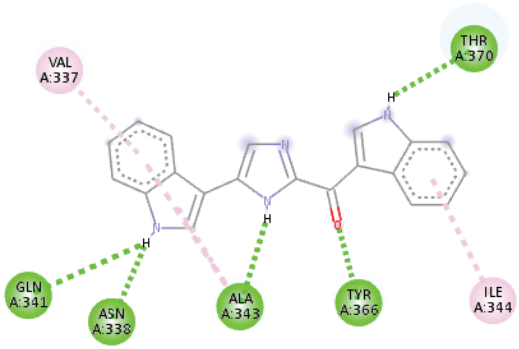

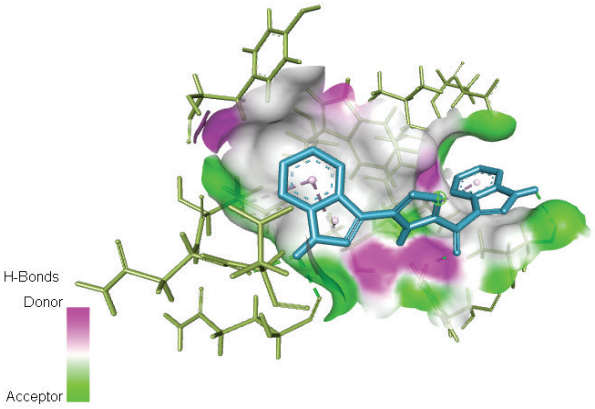

C

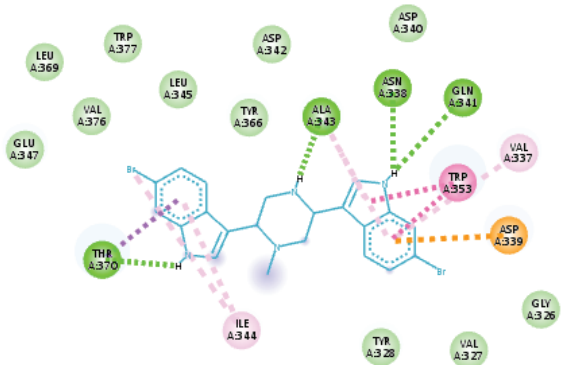

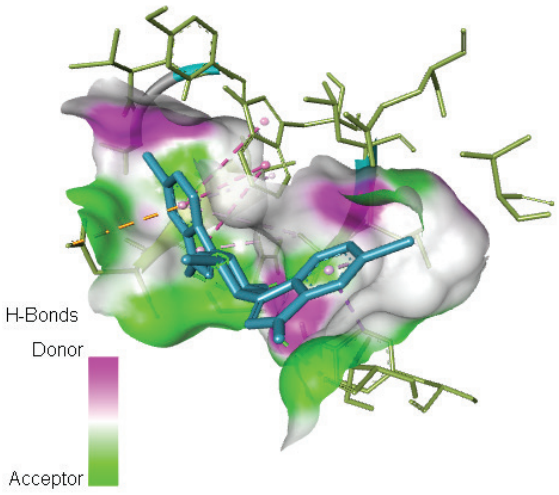

D

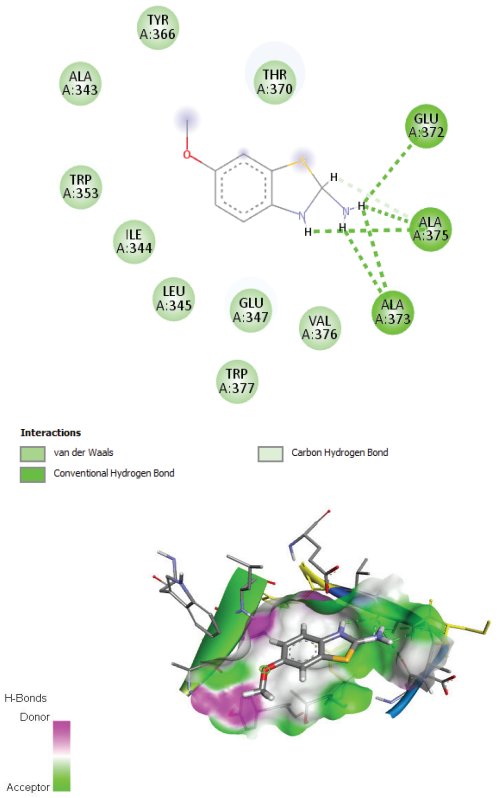

E

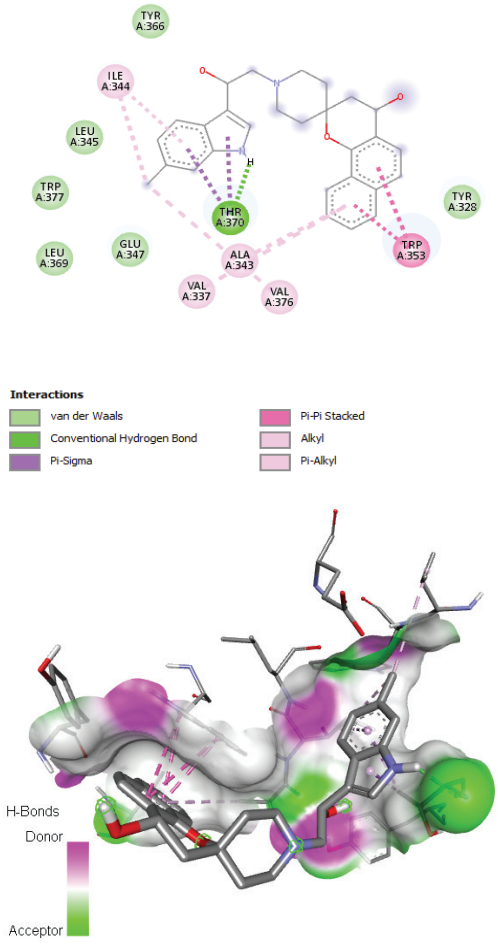

Figure 1: The 2D and 3D protein-ligand interactions of discorhabdin W – PHD (a); topsentin A – PHD (b); dragmacidin A – PHD (c); 6-methoxy-1,3-benzothiazol-2-amine – PHD (d); and JBC117 – PHD.

3.4 Molecular Dynamics Simulation

Molecular dynamics (MD) simulations were conducted to evaluate the stability of the protein-ligand complex. These simulations can detect changes in protein structure caused by ligand binding. The Root Mean Square Fluctuation (RMSF) profile for the PHD domain, obtained using CABS-flex, illustrate the flexibility of the amino acids (Figure 2). Higher RMSF values indicate greater flexibility, while lower values indicate restricted movement throughout the simulation.

Submitting the protein structure in PDB format to CABS-flex with default settings produces an output file containing 10 modeled structures and a graph showing each residue root-mean-square fluctuation (RMSF) (Figure 2). This analysis measures the movement within the protein/peptide complex. The PHD domain displayed the highest fluctuation of 3.053 Å and the lowest fluctuation of 0.152 Å.

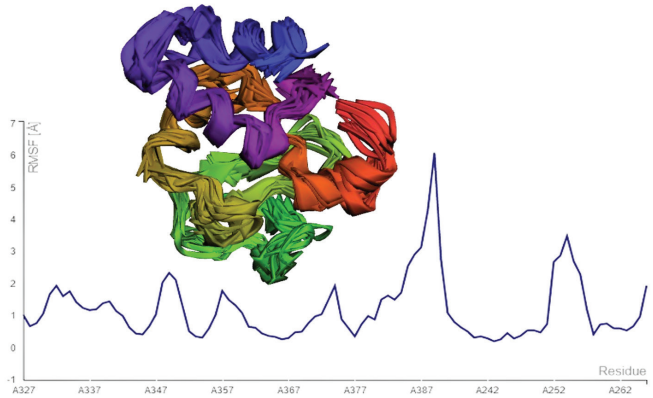

Figure 2: The multimodal superimposed simulated structure and molecular dynamics simulation depicting the RMSF profile of PHD.

To assess the stability and physical movements of the best three docked complexes, the researchers conducted molecular dynamics (MD) simulations using the iMOD server. The researchers employed normal mode analysis (NMA) to study the slow dynamics and large-scale conformational changes of the docked complexes. The results of NMA showing cluster movement for the PHD-discorhabdin W, PHD-dragmacidin A, and PHD-topsentin A complexes are shown in Figure 3.

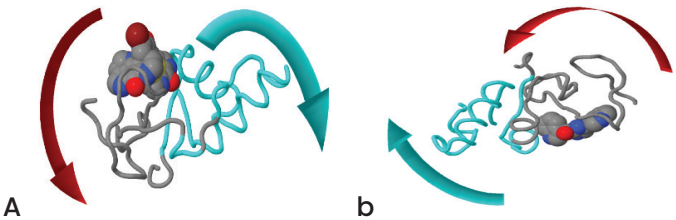

Advances in Medical, Pharmaceutical and Dental Research Journal (AMPDR)- ISSN 2812-4898
http://dx.doi.org/10.21622/AMPDR.2024.04.2.923

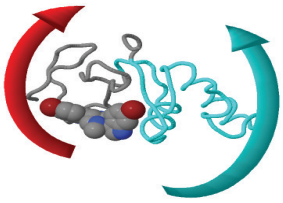

C

Figure 3: Molecular mobility evaluated by normal mode analysis (NMA) of the docked complexes: (A) PHD-discorhabdin W; (B) PHD-topsentin A; and (C) PHD-dragmacidin A. Distinct colors represent different clusters within the protein moiety, and colored affine arrows indicate the direction of motion, with longer arrows signifying greater motion.

The deformability and B-factor profiles indicate the mobility of the docked proteins. For the PHD-discorhabdin W, PHD-dragmacidin A, and PHD-topsentin A complexes, the deformability and B-factor graphs highlight the regions with the most significant movements, with the highest peaks representing areas of high deformability. These graphs also allow for a comparison between the normal mode analysis (NMA) and the PDB data of the complexes (Figures 4, 5 and 6)

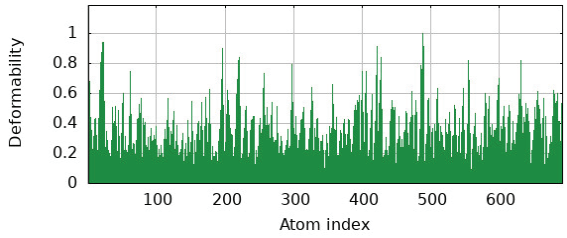

A

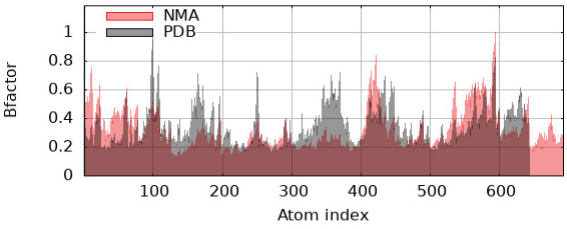

B

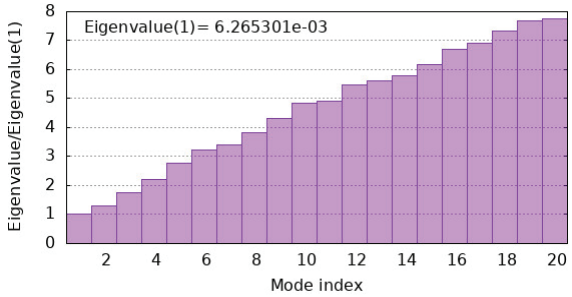

C

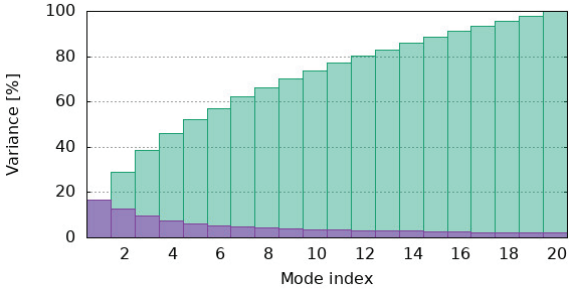

D

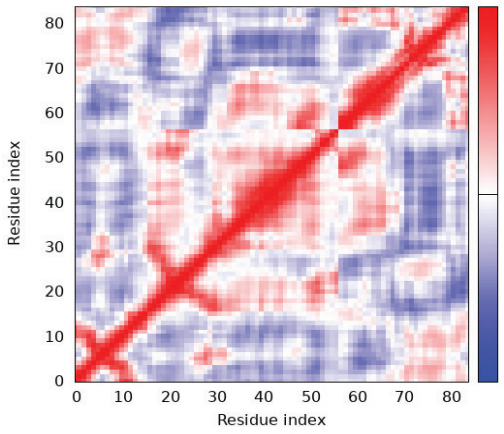

E

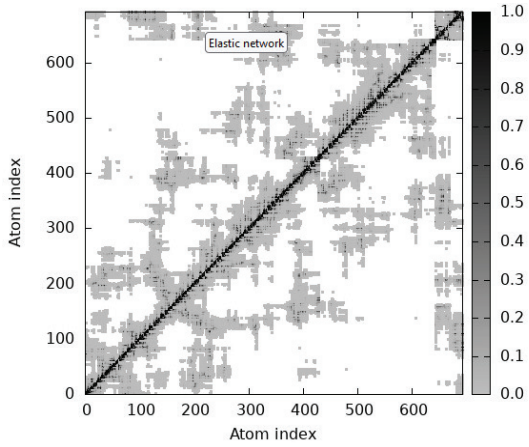

F

Figure 4: Results of molecular dynamics simulations in iMODS for PHD-discorhabdin W: (A) deformability; (B) B-factor plot; (C) eigenvalue; (D) variance plot; (E) covariance map; and (F) elastic network model.

Figures 4, 5, and 6 display the eigenvalues of the complexes. The docked complexes yielded eigenvalues of 6.265×10^{-3}, 6.216×10^{-3}, and 6.233×10^{-3} for discorhabdin W, dragmacidin, and topsentin A, respectively. The variance graph shows individual variance with purple bars and cumulative variance with green bars (Figures 4 and 5). In Figures 4 and 5, the covariance maps illustrate correlated motions between residue pairs in red, uncorrelated motions in white, and anti-correlated motions in blue. The elastic network maps highlight atom connections, with darker gray regions indicating stiffer areas (Figures 4, 5, and 5). From the molecular dynamics study of the PHD-discorhabdin W, PHD-dragmacidin A, and PHD-topsentin A docked complexes, it is evident that these complexes exhibited significant deformability (Figures 4, 5, and 6) and low eigenvalues. These low eigenvalues indicate easier deformability of the complex and also represent the stiffness of the protein complex.

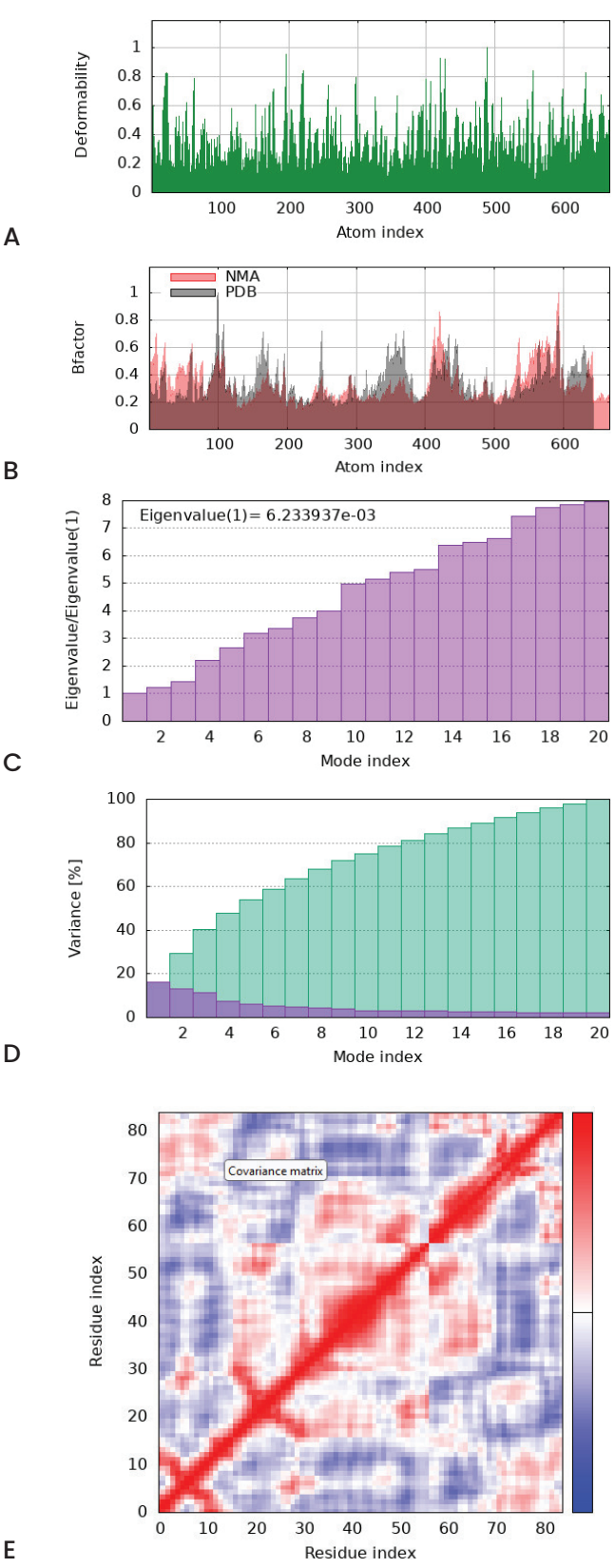

Figure 5: Results of molecular dynamics simulations in iMODS for PHD-topsentin A: (A) deformability; (B) B-factor plot; (C) eigenvalue; (D) variance plot; (E) covariance map; and (F) elastic network model.

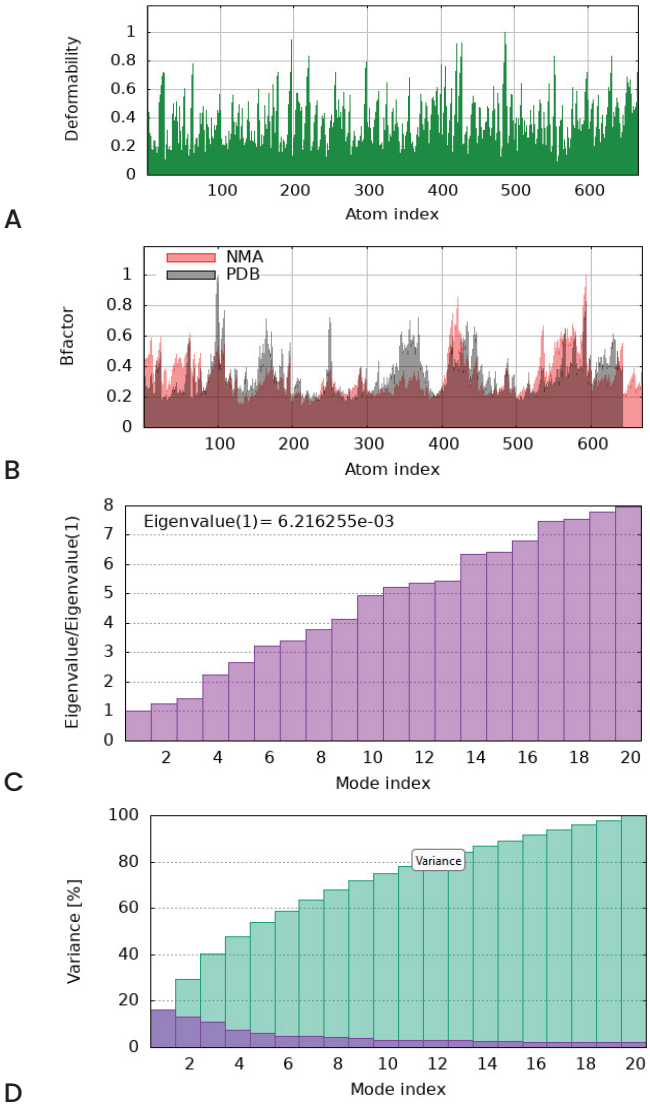

Advances in Medical, Pharmaceutical and Dental Research Journal (AMPDR)- ISSN 2812-4898
http://dx.doi.org/10.21622/AMPDR.2024.04.2.923

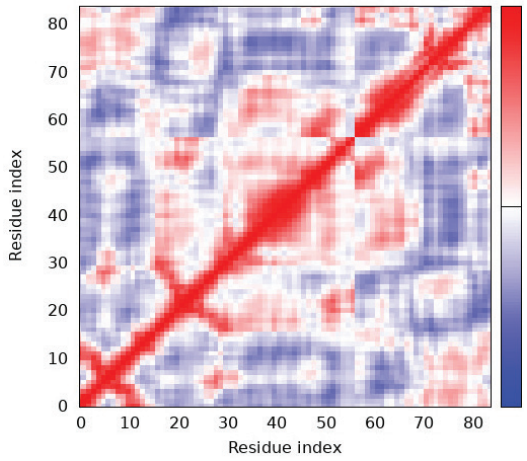

E

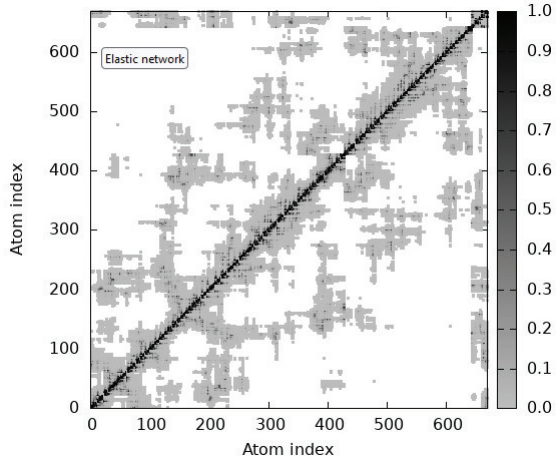

F

Figure 6: Results of molecular dynamics simulations in iMODS for PHD-dragmacidin A: (A) deformability; (B) B-factor plot; (C) eigenvalue; (D) variance plot; (E) covariance map; and (F) elastic network model.

4. DISCUSSION

The WNT signaling pathway, one of the most evolutionarily conserved pathways, plays a critical role in various biological processes, including embryonic development, cell proliferation, self-renewal, and cellular differentiation. Activation of the canonical WNT pathway leads to β-catenin-mediated transcriptional changes. In the absence of a WNT ligand, β-catenin is marked by the destruction complex for proteasomal degradation. However, WNT signaling prevents this degradation, allowing newly synthesized β-catenin to translocate to the nucleus and mediate transcription. In the nucleus, β-catenin interacts with transcription factors and co-activators such as BCL9 and PYGO, forming part of the WNT enhanceosome. These co-activators bind to the N-terminal domain of β-catenin, facilitating transcriptional regulation (41)

Targeting components of the WNT enhanceosome, specifically BCL9, PYGO etc. has shown therapeutic potential in cancer treatment. The PHD domain of Pygo2 is crucial for its binding to the N-terminal domain of β-catenin via adaptor proteins (41). Pygo2 recognizes modified histone 3 (H3K4me) tails through its PHD domain and interacts with the HD1 domain of BCL9, an adaptor protein directly binding β-catenin. This interaction is essential for β-catenin-dependent transcriptional switches in both normal and malignant tissues. The PHD domain pivotal role in Pygo2 function makes it a promising target for inhibiting the oncogenic functions of the β-catenin pathway (4). Knockdown of PYGO2 in human glioma cell lines results in decreased expression of WNT/β-catenin pathway targets, reducing tumor formation in chemically induced colon cancer and delaying mammary tumorigenesis in mice by inhibiting WNT signaling and reducing overexpression of target genes (42). Thus, pharmacologically targeting Pygo2's PHD domain could offer significant therapeutic benefits in cancers with β-catenin mutations.

Targeted therapy and molecular docking have transformed the development of advanced and potent anti-cancer drugs. Building on previous studies that demonstrated the anticancer properties of various alkaloidal ligands the researchers evaluated the binding energies of these alkaloids with the PHD domain of Pygo2 in this study. Our results indicate that discorhabdin W, topsentin A, and dragmacidin A exhibited the most favourable binding effect on the protein, with binding energies of -9.7, -9.1, and -9.0 Kcal/mol respectively among the ligands as shown in Table 1. Compounds with low binding energies are more likely to effectively inhibit their targets at lower concentrations, resulting in stronger inhibitory effects (43). Also, the selected binding pose for all the ligands had a root mean square deviation (rmsd) upper bound (ub) and lower bound (lb) values of 0.0. An rmsd of 0.0 signifies perfect alignment with the reference conformation, ensuring a highly accurate and reliable binding pose.

The top three ligands are marine alkaloids, highlighting the remarkable potential of marine organisms as sources of novel secondary metabolites with unique chemical structures and diverse pharmacological activities. These metabolites are pivotal in developing new drugs. Numerous studies have underscored the chemical uniqueness and bioactivity of latrunculid sponges. *Latrunculia* du Bocage, the largest genus in the family Latrunculiidae, comprises over 30 valid species divided into three subgenera: *Biannulata, Latrunculia*, and *Uniannulata*. Among these, *Latrunculia* is the most extensively studied subgenus in terms of chemical composition. Research on *Latrunculia* spp. has revealed various pyrroloiminoquinone-type alkaloids, commonly known as discorhabdins, which demonstrate significant bioactive potential (44).

Discorhabdin W, isolated from the deep marine sponge Latrunculia sp., is a symmetrical dimer of discorhabdin linked by a disulfide bond. (+)-Discorhabdin W, the first dimeric discorhabdin sourced from a New Zealand *Latrunculia* sp. collected from Milford Sound, exhibits anticancer potency against P388 lymphocytic leukemia cells with IC50 values of 0.084 μM. Additionally, (-)-Discorhabdin W, isolated from an Australian *Latrunculia* sp., showed activity in the HIF-1α/p300 interaction in a cell-free protein-protein assay (44). Mondal *et al.* (2019) noted that discorhabdin W exhibited superior anticancer activity compared to other discorhabdin compounds. These findings underscore the promising therapeutic properties of secondary metabolites from *Latrunculia* spp. and corroborate the exceptional binding affinity exhibited by discorhabdin W in the present study. Additionally, Casapullo *et al.* (2000) investigated the Mediterranean sponge *Rhaphisia lacazei* under the European project Bioactive Marine Natural Products, funded by the EU. A bioassay-guided fractionation of a crude extract led to the isolation of 13 bisindole alkaloids. The major metabolites including topsentins A, B1, and B2 were tested on the NSCLC-N6 carcinoma cell line, with B1 and B2 showing moderate cytotoxic activity (IC50: 12.0 and 6.3 μg/mL, respectively) (45). Although Topsentin A was not tested due to limited quantity, Prakash *et al.* (2015) noted that all three alkaloids exhibited antiproliferative activity against NSCLC-N6 cells. Lastly, dragmacidins, including dragmacidin A, isolated from *Dragmacidin* sp, and also a bis-indole alkaloid exhibit a broad spectrum of biological activities, with notable anticancer properties (22).

The interactions contributing to the superior binding effects of the best ligands on the PHD domain are depicted in the 2D and 3D diagrams of the protein-ligand complexes shown in Figures 1A to 1C. Hydrogen bonds, van der Waals forces, and various hydrophobic noncovalent interactions between ligands and proteins are crucial for the stability of complexes. The differing binding affinities of hit compounds and JBC117 are due to variations in bond type, chemical scaffolds, and amino acid residues involved in complex formation. The 1,4-dihydroindol-7-one of the pyrrolo [4,3,2- de]quinoline ring in discorhabdin W is a critical scaffold in both monomeric units of the dimer. It forms 5 conventional hydrogen bonds, 2 pi-pi stacked interactions, 3 pi-alkyl interactions, and 2 pi-anion bonds with the protein's amino acid residues, totaling 12 out of 16 interactions. The disulfide linkage also forms a pi-sulfur bond with the indole ring of tryptophan, enhancing the overall binding affinity. The oligomeric form of discorhabdin W is advantageous, allowing the pyrroloquinoline moiety, known for its strong antitumor effects across various cancer cell lines, to be represented twice. This multiplicity in bonding capacity explains the ligand's exceptional binding affinity.

Similarly, imidazole and indole rings are crucial in developing anticancer drugs. Both Topsentin A and Dragmacidin A are bis-indole alkaloids containing two indole moieties; however, Topsentin A includes an imidazole scaffold, which is absent in Dragmacidin A. As shown in Figures 1B and 1C, both alkaloids form three conventional hydrogen bonds with their indole rings and the same amino acid residues—polar uncharged GLN 341, ASN 338, and THR 370—accounting for their comparable binding affinities. Notably, Topsentin A has one additional hydrogen bond compared to Dragmacidin A, which interacts with the protein through several hydrophobic interactions. The extra hydrogen bond in Topsentin A underscores the role of hydrogen bonds in determining the affinity and specificity of protein-ligand interactions, possibly explaining the slight differences in binding affinities observed for both ligands (46). Madushanka *et al.* (2023) designed two pharmaceutically beneficial hydrogen bond databases, containing approximately 12,000 and 400 protein-ligand complexes, respectively, with around 22,000 and 2,200 hydrogen bonds. This study highlighted the significance of hydrogen bonds in protein-ligand binding affinity and selectivity, supporting our findings.

JBC117 contains a naphthalene ring, forming two pi-pi stacked interactions with the indole ring of TRP 353 and two pi-alkyl bonds with the aliphatic side chains of VAL 337 and ALA 343. Like the bis-indole alkaloids, JBC117 also has an indole ring (6-methyl-1H-indole) that forms a conventional hydrogen bond with the hydroxyl oxygen of THR 370 using its NH hydrogen. The THR 370 residue of the PHD domain is crucial for forming hydrogen bonds between the amine hydrogen of indole-containing alkaloids and the PHD finger. This observation supports Madushanka *et al.* (2023), establishing that N-H···O is the most frequent hydrogen bond type in their set of protein-ligand complexes. However, as seen in Figure 1E, this is the only hydrogen bond formed in the complex. Therefore, the high binding affinity observed here is largely due to other hydrophobic bond types formed by the various residues of the protein and parts of the alkaloid. Thus, as previously mentioned, the various types of bonds, residues involved, differing bond strengths, and chemical scaffolds contribute to the observed variations in binding affinities of the complexes in this study.

Ali *et al.* (2016) identified the binding sites between JBC117 and the PHD domain, which include ASP 339 (located at the K4me pocket of the PHD), ALA 348, VAL 376, and ALA 378 (located at the PHD–HD1 interface). The 2D representation of the PHD-discorhabdin W complex shows that discorhabdin W interacts with ASN 338, a residue near ASP 339, via a conventional hydrogen bond. Topsentin A and dragmacidin A interact with the PHD domain at

Advances in Medical, Pharmaceutical and Dental Research Journal (AMPDR)- ISSN 2812-4898
http://dx.doi.org/10.21622/AMPDR.2024.04.2.923

VAL 337 and ASN 338 via pi-alkyl and conventional hydrogen bonds, respectively. Additionally, discorhabdin W binds with GLU 347, near ALA 348, via pi-anion bonds, and with ALA 375, close to VAL 376 and ALA 378, via conventional hydrogen bonds. However, dragmacidin A binds exactly with ASP 339, as Ali *et al*., (2016) observed for JBC117 via a pi-anion bond. This underscores the importance of the ASP 339 residue in binding the protein with ligands. The proximity of these binding residues suggests that the interaction between the ligands and the PHD domain may influence histone binding as well as the interaction between PHD and HD1 just like JBC117. However, further evaluations, including heteronuclear single quantum coherence (HSQC) NMR, are needed to confirm this hypothesis.

The reached results also demonstrated that while Topsentin A and dragmacidin A inhibit all CYP isoforms except CYP2C9, Discorhabdin W inhibits none except CYP2C9 as shown in Table 3. It is well-established that the broader the spectrum of CYP isoforms inhibited by a small molecule, the higher the potential for drug-drug interactions with a wide range of other medications (47). Therefore, topsentin A and dragmacidin A, which inhibit four isoforms, have a higher likelihood of causing side effects or adverse drug reactions. Conversely, Discorhabdin W is less likely to induce such effects. Therefore, it is very important to control the use of topsentin A and dragmacidin A to prevent the side effects of their use.

The toxicity test depicted in Table 3 revealed that dragmacidin A, topsentin A, and discorhabdin W have an LD50 value of 313 mg/kg, 1264 mg/kg, and 6000mg/kg, respectively. They also belong to toxicity classes, 4, 4, and 6 respectively. Karaduman and Kelleci çelik (2022) emphasize that the accurate calculation of the LD50/LC50 value is essential for ensuring the safe use of medications and predicting potential adverse reactions. This measurement aids in establishing the drug toxicity profile (48)rendering it a valuable tool in the early stages of drug development. Dragmacidin A falls into the slightly toxic category. Its LD50 value suggests that careful dosage management is necessary to avoid adverse effects. Topsentin A also belongs to class 4 but with a higher LD50 value indicating lower toxicity compared to dragmacidin A. This suggests a wider safety margin for therapeutic use, making it potentially safer at higher doses. However, discorhabdin W is classified as non-toxic.

Its high LD50 value implies minimal risk of acute toxicity even at relatively high doses, making it the safest of the best three alkaloids for therapeutic use. Additionally, for organ toxicity, only topsentin A of the best three ligands shows a propensity for hepatotoxicity, indicating a potential risk for drug-induced liver injury, which can manifest as acute or chronic liver damage with varying clinical presentations and mechanisms (49). Furthermore, cardiotoxicity, particularly hERG-related cardiotoxicity, is a significant concern with anti-cancer drugs due to its potential to induce arrhythmias, cardiac contractile dysfunction, coronary artery disease, and hypertension, impacting the quality of life for cancer patients (50). The results obtained showed that topsentin A has the least probability of inhibiting the hERG potassium ion channels, while dragmacidin A has a relatively high probability to inhibit the hERG potassium ion channel. These channels are crucial for the electrical activity of the heart, specifically in the repolarization phase of the cardiac action potential. Inhibiting these channels may lead to prolonged QT intervals on an electrocardiogram, increasing the risk of arrhythmias such as Torsades de Pointes which can be life threatening (51). Therefore, comprehensive preclinical and clinical studies are necessary to confirm the safety of these alkaloids.

Through the MD simulation assessment of the protein using CABS-flex, the researchers observed several regions with high flexibility, indicated by RMSF peaks, Figure 2. A higher RMSF value signifies more flexible movements, while a lower RMSF value indicates restricted movements from the average position during the simulation (52). CABS-flex calculates RMSF from 10 ns simulations of the protein/peptide, focusing on small-timescale dynamics with the default set of parameters and restraints. Additionally, the CABS-flex study produced RMSFs comparable to those obtained from NMR Ensemble RMSFs (53). Thus, the binding of the best three ligands with the PHD domain could influence the mechanisms involved in the β-catenin-dependent transcriptional regulation in malignant tissues.

Flexibility plays a crucial role in interacting biological macromolecules with substrates or in protein-protein interactions (54). iMODS is a rapid and straightforward server for defining and calculating protein flexibility. It analyzes molecular motion and structural flexibility using Normal Mode Analysis (NMA), which incorporates coordinates from docked complexes (55). NMA of proteins assumes that the vibrational normal modes with the minimum frequencies correspond to the largest movements in a protein, which are functionally significant (56). The NMA study of the docked complexes revealed substantial mobility, confirming their structural flexibility.

Furthermore, the findings indicated significant deformability in the protein, with various peaks observed in the deformability index, approximately 1.0, Figures 4A, 5A, and 6A. Deformability measures the flexibility of a protein, while the B-factor reflects its mobility (57). Regions showing significant peaks

in both NMA and PDB B-factors are potential hinge regions, indicating flexibility in both experimental and theoretical models. Analysis of B-factors for PHD-discorhabdin W, PHD-dragmacidin A, and PHD-topsentin A highlighted significant hinge regions, demonstrating consistency between theoretical and experimental models, Figures 4B, 5B, and 6B.

The eigenvalues computed for the three docked complexes are directly related to the energy required to deform its structure, indicating the motion stiffness of the protein-ligand complex. A lower eigenvalue suggests easier deformability of the complex (27). This molecular dynamics study of the docked complexes revealed significant deformability, with the three complexes exhibiting low eigenvalues, indicating stable and flexible molecular motions. The variance maps of the three complexes produced reasonable results. The covariance matrices indicated strong correlations and anticorrelations. The elastic maps also provided reasonable results.

5. CONCLUSION

Through docking studies of alkaloids from various classes, the researchers identified three compounds, Discorhabdin W, dragmacidin A, and Topsentin A, with PHD domain binding affinities of -9.7 Kcal/mol, 9.1 Kcal/mol, and -9.1 Kcal/mol respectively, compared to JBC117 (-9.2 Kcal/mol), a compound known to bind the PHD domain and exhibit anti-proliferative activity in cancer cells both ex vivo and in vivo. Given the favourable interactions and drug-like characteristics of these top three ligands with the PHD domain, the researchers suggest they could be promising candidates for selectively targeting the Pygo-BCL9 interface, thereby potentially inhibiting the oncogenic Wnt pathway. However, further investigations are needed in vivo to optimize their chemical structures and assess their pharmacokinetics, pharmacodynamics, and safety profiles to advance their potential as drug candidates.

Acknowledgements:
The researchers gratefully acknowledge the ICT unit of Lagos State University for providing complimentary internet access and technical support for this work.

Conflict of Interest:
The authors declare no conflicts of interest.

6. REFERENCES

1. Clevers H, Nusse R. Wnt/β-catenin signaling and disease. Vol. 149, Cell. 2012.
2. Polakis P. Wnt signaling in cancer. Cold Spring Harb Perspect Biol. 2012;4(5).
3. Miller TCR, Rutherford TJ, Johnson CM, Fiedler M, Bienz M. Allosteric Remodelling of the Histone H3 Binding Pocket in the Pygo2 PHD Finger Triggered by Its Binding to the B9L/BCL9 Co-Factor. J Mol Biol. 2010;401(5).
4. Ali F, Yamaguchi K, Fukuoka M, Elhelaly AE, Kuwata K. Logical design of an anti-cancer agent targeting the plant homeodomain in Pygopus2. Cancer Sci. 2016;107(9).
5. Zhu Y, Zhao Y, Wen J, Liu S, Huang T, Hatial I, et al. Targeting the chromatin effector Pygo2 promotes cytotoxic T cell responses and overcomes immunotherapy resistance in prostate cancer. Sci Immunol. 2023;8(81).
6. Kramps T, Peter O, Brunner E, Nellen D, Froesch B, Chatterjee S, et al. Wnt/Wingless signaling requires BCL9/legless-mediated recruitment of pygopus to the nuclear β-catenin-TCF complex. Cell. 2002;109(1).
7. Gu B, Sun P, Yuan Y, Moraes RC, Li A, Teng A, et al. Pygo2 expands mammary progenitor cells by facilitating histone H3 K4 methylation. Journal of Cell Biology. 2009;185(5).
8. Olawale F, Iwaloye O, Olofinsan K, Ogunyemi OM, Gyebi GA, Ibrahim IM. Homology modelling, vHTS, pharmacophore, molecular docking and molecular dynamics studies for the identification of natural compound-derived inhibitor of MRP3 in acute leukaemia treatment. Chemical Papers. 2022;76(6).
9. Olofinsan K, Abrahamse H, George BP. Therapeutic Role of Alkaloids and Alkaloid Derivatives in Cancer Management. Vol. 28, Molecules. 2023.
10. Wang X, Tanaka M, Krstin S, Peixoto HS, Wink M. The interference of selected cytotoxic alkaloids with the cytoskeleton: An insight into their modes of action. Molecules. 2016;21(7).
11. Jash C, Kumar GS. Binding of alkaloids berberine, palmatine and coralyne to lysozyme: A combined structural and thermodynamic study. RSC Adv. 2014;4(24).
12. Bhuiya S, Pradhan AB, Haque L, Das S. Molecular Aspects of the Interaction of Iminium and Alkanolamine Forms of the

Advances in Medical, Pharmaceutical and Dental Research Journal (AMPDR)- ISSN 2812-4898
http://dx.doi.org/10.21622/AMPDR.2024.04.2.923

Anticancer Alkaloid Chelerythrine with Plasma Protein Bovine Serum Albumin. Journal of Physical Chemistry B. 2016;120(1).

13. Khan AY, Suresh Kumar G. Natural isoquinoline alkaloids: binding aspects to functional proteins, serum albumins, hemoglobin, and lysozyme. Vol. 7, Biophysical Reviews. 2015.

14. Katyal P, Sharma S. Emerging Alkaloids Against Cancer: A Peep into Factors, Regulation, and Molecular Mechanisms. In: Bioactive Natural Products for the Management of Cancer: from Bench to Bedside. 2019.

15. Vishesh Verma, Shivam Sharma, Kritika Gaur, Nitin Kumar. Role of vinca alkaloids and their derivatives in cancer therapy. World Journal of Advanced Research and Reviews. 2022;16(3).

16. Sousa-Pimenta M, Estevinho LM, Szopa A, Basit M, Khan K, Armaghan M, et al. Chemotherapeutic properties and side-effects associated with the clinical practice of terpene alkaloids: paclitaxel, docetaxel, and cabazitaxel. Vol. 14, Frontiers in Pharmacology. 2023.

17. Rahman N, Muhammad I, Nayab GE, Khan H, Aschner M, Filosa R, et al. Molecular Docking of Isolated Alkaloids for Possible α-Glucosidase Inhibition. Biomolecules. 2019;9(10).

18. Shahik SM, Salauddin A, Hossain MS, Noyon SH, Moin AT, Mizan S, et al. Screening of novel alkaloid inhibitors for vascular endothelial growth factor in cancer cells: An integrated computational approach. Genomics Inform. 2021;19(1).

19. Mondal A, Gandhi A, Fimognari C, Atanasov AG, Bishayee A. Alkaloids for cancer prevention and therapy: Current progress and future perspectives. Vol. 858, European Journal of Pharmacology. 2019.

20. Rose W. Peter, Prlić Andreas, Altunkaya Ali, Bi Chunxiao, Bradley R. Anthony, Christie Coleh H. The RCSB protein data bank: integrative view of protein, gene and 3D structural information. 2016;45.

21. Kanmodi R, Oddiri R, Arowosegbe M, Rahmon S. Exploring the pharmacokinetic properties and inhibitory potentials of plant-derived alkaloids against nuclear protein targets in triple-negative breast cancer: An In Silico approach. Sci Afr. 2023;22.

22. Gupta AP, Pandotra P, Kushwaha M, Khan S, Sharma R, Gupta S. Alkaloids: A source of anticancer agents from nature. In: Studies in Natural Products Chemistry. 2015.

23. Kim S, Thiessen PA, Bolton EE, Chen J, Fu G, Gindulyte A, et al. PubChem substance and compound databases. Nucleic Acids Res. 2016;44(D1).

24. Lobo S. Is there enough focus on lipophilicity in drug discovery? Vol. 15, Expert Opinion on Drug Discovery. 2020.

25. Azzam K AL. SwissADME and pkCSM Webservers Predictors: an integrated Online Platform for Accurate and Comprehensive Predictions for In Silico ADME/T Properties of Artemisinin and its Derivatives. Kompleksnoe Ispol'zovanie Mineral'nogo syr'â/Complex Use of Mineral Resources/Mineraldik Shikisattardy Keshendi Paidalanu [Internet]. 2023 Jun 15 [cited 2024 Sep 2];325(2):14–21. Available from: http://kims-imio.com/index.php/main/article/view/252/322

26. Banerjee Priyanka, Kemmler Emanuel, Dunkel Mathias, Preissner Robert. ProTox 3.0: a webserver for the prediction of toxicity of chemicals .

27. Sumera, Anwer F, Waseem M, Fatima A, Malik N, Ali A, et al. Molecular Docking and Molecular Dynamics Studies Reveal Secretory Proteins as Novel Targets of Temozolomide in Glioblastoma Multiforme. Molecules. 2022;27(21).

28. Roessler HI, Knoers NVAM, van Haelst MM, van Haaften G. Drug Repurposing for Rare Diseases. Vol. 42, Trends in Pharmacological Sciences. 2021.

29. Deyá AD. ANTI-CANCER PROPERTIES OF BENZOPHENANTHRIDINE ALKALOIDS FROM Zanthoxylum genus - in silico EVIDENCE. Rev Latinoam Quim. 2022;49(1).

30. Daina A, Michielin O, Zoete V. SwissADME: A free web tool to evaluate pharmacokinetics, drug-likeness and medicinal chemistry friendliness of small molecules. Sci Rep. 2017;7.

31. Ongtanasup T, Mazumder A, Dwivedi A, Eawsakul K. Homology Modeling, Molecular Docking, Molecular Dynamic Simulation, and Drug-Likeness of the Modified Alpha-Mangostin against the β-Tubulin Protein of Acanthamoeba Keratitis. Molecules. 2022;27(19).

32. Chancellor MB, Staskin DR, Kay GG, Sandage BW, Oefelein MG, Tsao JW. BloodBrain barrier permeation and efflux exclusion of anticholinergics used in the treatment of

overactive bladder. Vol. 29, Drugs and Aging. 2012.

33. Testa Bernard, Krämer Stefanie D. The Biochemistry of Drug Metabolism – An Introduction. 2008;

34. Di L. The role of drug metabolizing enzymes in clearance. Vol. 10, Expert Opinion on Drug Metabolism and Toxicology. 2014.

35. Lamb DC, Waterman MR, Kelly SL, Guengerich FP. Cytochromes P450 and drug discovery. Vol. 18, Current Opinion in Biotechnology. 2007.

36. Kirchmair J, Göller AH, Lang D, Kunze J, Testa B, Wilson ID, et al. Predicting drug metabolism: Experiment and/or computation? Vol. 14, Nature Reviews Drug Discovery. 2015.

37. Rathod S, Desai H, Patil R, Sarolia J. Non-ionic Surfactants as a P-Glycoprotein(P-gp) Efflux Inhibitor for Optimal Drug Delivery—A Concise Outlook. Vol. 23, AAPS PharmSciTech. 2022.

38. Lipinski CA, Lombardo F, Dominy BW, Feeney PJ. Experimental and computational approaches to estimate solubility and permeability in drug discovery and development settings. Vol. 23, Advanced Drug Delivery Reviews. 1997.

39. Ya'u Ibrahim Z, Uzairu A, Shallangwa G, Abechi S. Molecular docking studies, drug-likeness and in-silico ADMET prediction of some novel β-Amino alcohol grafted 1,4,5-trisubstituted 1,2,3-triazoles derivatives as elevators of p53 protein levels. Sci Afr. 2020;10.

40. Miller TCR, Rutherford TJ, Birchall K, Chugh J, Fiedler M, Bienz M. Competitive binding of a benzimidazole to the histone-binding pocket of the pygo PHD finger. ACS Chem Biol. 2014;9(12).

41. Groenewald W, Lund AH, Gay DM. The Role of WNT Pathway Mutations in Cancer Development and an Overview of Therapeutic Options. Vol. 12, Cells. 2023.

42. Esposito I, Cassaro A. PYGO2 (pygopus family PHD finger 2). Vol. 24, Atlas of Genetics and Cytogenetics in Oncology and Haematology. 2020.

43. Umamaheswari M, Aji CS, Asokkumar K, Sivashanmugam T, Subhadradevi V, Jagannath P, et al. Docking studies: In silico aldose reductase inhibitory activity of commercially available flavonoids. Bangladesh J Pharmacol. 2012;7(2).

44. Li F, Kelly M, Tasdemir D. Chemistry, chemotaxonomy and biological activity of the latrunculid sponges (Order poecilosclerida, family latrunculiidae). Vol. 19, Marine Drugs. 2021.

45. Casapullo A, Bifulco G, Bruno I, Riccio R. New bisindole alkaloids of the topsentin and hamacanthin classes from the Mediterranean marine sponge Rhaphisia lacazei. J Nat Prod. 2000;63(4).

46. Madushanka A, Moura RT, Verma N, Kraka E. Quantum Mechanical Assessment of Protein–Ligand Hydrogen Bond Strength Patterns: Insights from Semiempirical Tight-Binding and Local Vibrational Mode Theory. Int J Mol Sci. 2023;24(7).

47. Cheng F, Yu Y, Zhou Y, Shen Z, Xiao W, Liu G, et al. Insights into molecular basis of cytochrome P450 inhibitory promiscuity of compounds. J Chem Inf Model. 2011;51(10).

48. Karaduman G, Kelleci Çelik F. A MULTIVARIATE INTERPOLATION APPROACH FOR PREDICTING DRUG LD50 VALUE. Ankara Universitesi Eczacilik Fakultesi Dergisi. 2024;48(1).

49. Francis P, Navarro VJ. Drug Induced Hepatotoxicity. StatPearls Publishing; 2022.

50. Pawar Vinayak, Wankhede Yogesh, Kaur Simranjit, Pawar Bhakti, Vasdev Nupur, Gupta Tanisha. Drug-induced cardiotoxicity. Advances Pharmaceutical Product Development and Research. 2024;2.

51. Gintant G. An evaluation of hERG current assay performance: Translating preclinical safety studies to clinical QT prolongation. Vol. 129, Pharmacology and Therapeutics. 2011.

52. Kumar CV, Swetha RG, Anbarasu A, Ramaiah S. Computational analysis reveals the association of threonine 118 methionine mutation in PMP22 resulting in CMT-1A. Adv Bioinformatics. 2014;2014.

53. Jamroz M, Kolinski A, Kmiecik S. CABS-flex predictions of protein flexibility compared with NMR ensembles. Bioinformatics. 2014;30(15).

54. Ghosh P, Bhakta S, Bhattacharya M, Sharma AR, Sharma G, Lee SS, et al. A Novel Multi-Epitopic Peptide Vaccine Candidate Against Helicobacter pylori: In-Silico Identification, Design, Cloning and Validation Through Molecular Dynamics. Int J Pept Res Ther. 2021;27(2).

Advances in Medical, Pharmaceutical and Dental Research Journal (AMPDR)- ISSN 2812-4898
http://dx.doi.org/10.21622/AMPDR.2024.04.2.923

55. López-Blanco JR, Aliaga JI, Quintana-Ortí ES, Chacón P. IMODS: Internal coordinates normal mode analysis server. Nucleic Acids Res. 2014;42(W1).

56. Yao XQ, Skjærven L, Grant BJ. Rapid Characterization of Allosteric Networks with Ensemble Normal Mode Analysis. Journal of Physical Chemistry B. 2016;120(33).

57. Kovacs JA, Chacón P, Abagyan R. Predictions of protein flexibility: First-order measures. Proteins: Structure, Function and Genetics. 2004;56(4).